Full Paper

AUTOMATIC MEASUREMENT OF CT NUMBER LINEARITY IN THREE TYPES OF CATPHAN PHANTOMS

Choirul Anam[a*], Riska Amilia[a], Ariij Naufal[a], Geoff Dougherty[b]

[a]Department of Physics, Faculty of Sciences and Mathematics, Diponegoro University, 50275, Central Java, Indonesia
[b]Department of Applied Physics and Medical Imaging, California State University Channel Islands, Camarillo, CA 93012, USA

*Corresponding author
anam@fisika.fsm.undip.ac.id*

Graphic abstract
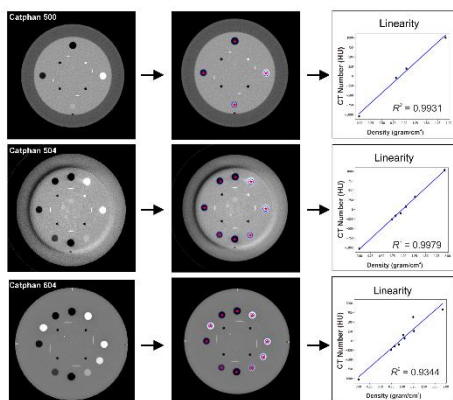
Abstract

This study aims to develop an algorithm for automatically measuring CT number linearity in three different types of Catphan phantom. We used a sensitometry module image from three Catphan phantoms (types 500, 504, and 604). Each phantom and its air material were segmented. Based on the centroid of the air material, the coordinates for every object within the sensitometry modules were determined. The average CT numbers for every object were calculated and graphs of CT number linearity were automatically generated. Accurate segmentation of each object in the sensitometry modules produced accurate graphs of CT number linearity for each phantom. The linear regression of the Catphan 604 failed to pass the tolerance level, while the other two phantoms passed with R2 > 0.99. The automatic CT number linearity measurements were easy, fast, and more objective than manual measurements.

Keywords: CT number linearity, Catphan phantom, CT scan, image quality

1.0 INTRODUCTION

The use of computed tomography (CT) for diagnosing disease has increased rapidly [1-5]. CT scans utilize X-ray radiation to generate patient images [6, 7]. Each tissue has a unique X-ray attenuation coefficient [8-10]. The different attenuations result in a variation of pixel values in the CT image. Pixel values in the images are converted to CT numbers in Hounsfield units (HU) [11-13].

The CT number has a paramount role in diagnosis with quantitative computed tomography (QCT) [14-16]. For example, QCT has been widely used to diagnose patients with anaemia. An abnormality is identified by comparing the attenuation of blood in a non-contrast examination with the attenuation of the

adjacent vessel wall or myocardium [17-19]. QCT is also widely used for the early detection of asymptomatic coronary heart disease with the Agatston score method [20, 21]. Recently, QCT has played a significant role in diagnosing patients with COVID-19 pneumonia [22-24]. It is vitally important to ensure the accuracy of the CT numbers to avoid misdiagnosis [25].

One way to ensure the accuracy of the CT numbers is to conduct a CT number linearity test, i.e. by evaluating the relationship between the CT number and the density of the material being imaged [26, 27]. The testing must be carried out periodically, since the CT number linearity is prone to alter within a specific period [28,29]. Various phantoms can be used for this testing, including the ACR phantom [30,31], the AAPM phantom [32,33], and the Catphan phantom [34-36].

For the Catphan phantom, there are many applications available to automatically perform the CT number linearity tests, such as Smari [37], AutoQA Plus [38], QA Master [39], QA Pilot [40], and CTQI [41], although some of these applications can only be used on certain types of Catphan phantom. However, they all require the phantom to be positioned at the iso-center. They cannot accurately measure CT numbers of objects within the phantom if there is slight mis-alignment or rotation of the phantom. This study aims to develop an algorithm to automatically measure CT number linearity on three different types of Catphan phantoms, even when the phantoms are not properly located at the iso-center.

2.0 METHODOLOGY

2.1 Catphan Phantom Images

A method to automatically measure the CT number linearity was applied to three types of Catphan phantom, i.e., Catphan 500, Catphan 504, and Catphan 604. The Catphan® phantoms were manufactured by Phantom Laboratory, Salem, New York, USA. Each phantom consists of several modules to test many image qualities. The CT number linearity test was carried out by scanning module #1 for CTP 500 and CTP 504 and #2 for CTP 604, as shown in Figure 1. The tests were performed with circular sensitometry objects in the edge area of the phantoms. Each phantom has a different number of sensitometry objects. CTP 500 has four objects: air, Teflon, acrylic, and LDPE. CTP 504 consists of eight objects with two circular air objects and Teflon, Delrin™, acrylic, polystyrene, low density polyethylene (LDPE), and polymethylpentene (PMP) objects. CTP 604 has the same eight objects as CTP 504 and two additional objects, namely bone-50% and bone-20%. The phantoms were positioned at their iso-centers on the table and scanned with the parameters tabulated in Table 1.

It is important to note that the sensitometry modules do not only contain objects for measuring CT number linearity. However, in this study, all objects other than those for measuring CT number linearity were not considered.
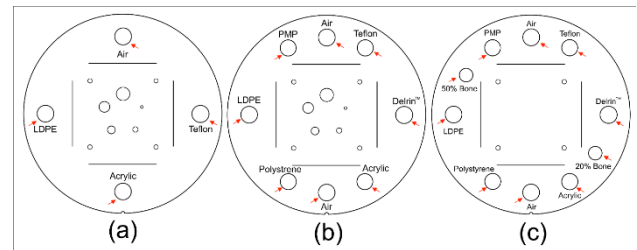
Figure 1 Schematic of Catphan phantom modules for measuring CT number linearity: (a) Catphan 500, (b) Catphan 504, and (c) Catphan 604. Objects for measuring CT number linearity are indicated by arrows

Table 1 Exposure parameters for scanning each Catphan phantom in this study

| Parameter	Phantom type		
	Catphan 500	Catphan 504	Catphan 604
Scanner	Siemens Somatom Definition AS+	Varian OBI CBCT	GE Medical Revolution
Tube voltage (kV)	120	120	120
Tube current (mA)	86	80	340
Field of view (mm)	250	250	250
Slice thickness (mm)	2.0	2.5	5.0
Revolution time (s)	1.0	1.0	1.0
Kernel	UB	Ram-Lak	Standard
Scan mode	Axial	Axial	Helical

2.2 CT Number Linearity

The CT number linearity was measured automatically from phantom images using a modification of a previous algorithm used for an ACR phantom [42]. It uses the segmentation-rotation method [43].

There are several stages in measuring the CT number linearity on a Catphan phantom (Figure 2). First, the phantom was segmented and its centroid was determined. Then, the air object within the phantom was segmented. The air object was chosen because it was the easiest to segment since the CT number difference with the background is around 1000 HU. In the CTP 504 and CTP 604 Phantoms, we used the air object located at the 12 o'clock position. The centers of the phantom and air object were used as references to determine the coordinates of the other objects.

The next step was to rotate the coordinates with a specific angle with respect to the centroid of the air object. The magnitude of the rotation angle used in each phantom was unique and is shown in Table 2. After the center coordinates of each material were obtained, ROIs with a radius of 12 pixels around each object were created and the average CT numbers within each ROI were calculated. Graphs of CT number vs. the density of each object were plotted. To pass the CT number linearity test R^2 should be greater than 0.99 [44].

**Table 2** Rotation angle for obtaining coordinates of objects

Object	Angle (°)		
	Catphan 500	Catphan 504	Catphan 604
Teflon	90	30	30
Acrylic	180	150	150
LDPE	270	270	270
Air	-	180	180
Delrin™	-	90	90
Polystyrene	-	210	210
PMP	-	330	330
Bone-50%	-	-	120
Bone-20%	-	-	300
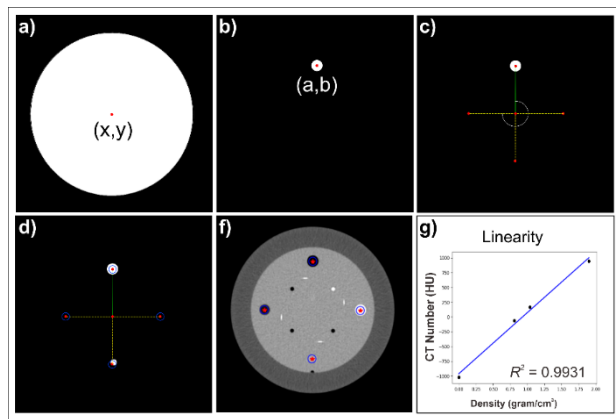
Figure 2 Steps of an automatic measurement of CT number linearity in the Catphan 500. (a) result of phantom segmentation and its centroid, (b) result of air object segmentation and its centroid, (c) rotating coordinate with reference of the centroids of phantom and air object. The centroid coordinates of the air object were rotated by 90°, 180°, and 270° to acquire the center coordinates of Teflon, acrylic, and LDPE, respectively, (d) creating ROIs around each objects, (e) calculation of the average CT number within each ROI of all objects, and (f) plotting the graph of the CT number linearity

3.0 RESULTS AND DISCUSSION

The segmentation results on the three Catphan phantoms are shown in Figure 3. Our software was successful in automatically segmenting all objects in the three different types of phantoms. The ROIs were accurately located within each object for each phantom. The CT numbers of each object are tabulated in Table 3. The results show that the CT number of most of the objects, except the Teflon objects, were within the reference range. However, the CT numbers of Teflon in Catphan 500 and Catphan 604 were below the range, and its value in Catphan 504 was above the range. The CT numbers of Delrin™ and Bone-20% were also out of the recommended range. The CT number of Delrin™ in Catphan 504 and Catphan 604 were 413.5 HU and 317.2 HU, respectively, while the CT number of Bone-20% in Catphan 604 was 208.7 HU. The CT numbers of the water, PMP, LDPE, polystyrene, and acrylic objects were all within the recommended range.
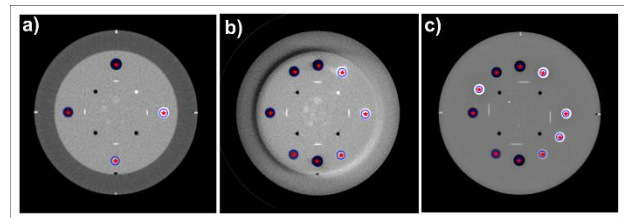
Figure 3 Automatic objects segmentation results for the three different types of Catphan phantom: (a) Catphan 500, (b) Catphan 504, and (c) Catphan 604

Figure 4 shows the graphs of CT number linearity for the three Catphan phantoms. Two of the phantoms, i.e. Catphan 500 and Catphan 504, passed the CT number linearity tolerance test with R^2 values greater than 0.99, but the Catphan 604 failed to pass the tolerance level.
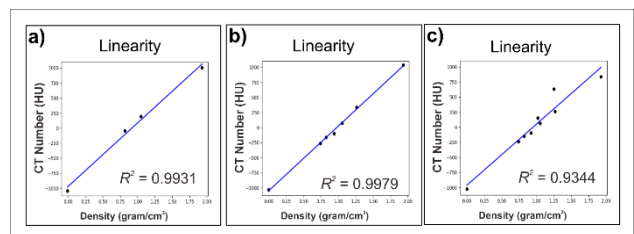
Figure 4 Graphs of CT number linearity for the three Catphan phantoms: (a) Catphan 500, (b) Catphan 504, and (c) Catphan 604

Table 3 Measured CT number from each object in the three different types of Catphan phantom

Object	Density (gram/cm³)	CT number reference (HU)	Measured CT number (HU)			CT number difference to the middle of reference (HU)		
			Catphan 500	Catphan 504	Catphan 604	Catphan 500	Catphan 504	Catphan 604
Air	0.00	-1046 to -986	-983.9	-998.9	-998.2	-32.1	17.1	17.8
PMP	0.83	-220 to -172	-	-203.6	-187.4	-	7.6	8.6
LDPE	0.92	-121 to -87	-88.8	-101.3	-98.3	-15.2	5.7	5.7
Polystyrene	1.03	-65 to -29	-	-36.1	-42.4	-	10.9	4.6
Acrylic	1.18	92 to 137	126.2	145.5	118.3	-11.7	31	3.8
Bone-20%	1.14	211 to 263	-	-	208.7	-	-	28.3
Delrin™	1.42	344 to 387	-	413.5	317.2	-	48	48.3
Bone-50%	1.40	667 to 783	-	-	692.9	-	-	32.1
Teflon	2.16	941 to 1060	854.0	1136.8	903.2	146.5	136.3	97.3

The CT numbers presented in a CT image are widely used for diagnosing diseases in patients, e.g., anemia, coronary heart disease, and pulmonic. The CT number linearity test evaluates whether the CT numbers in an image correspond to the tissue densities of the objects or not. The current study aimed to develop an algorithm that could automatically measure CT number linearity on three types of Catphan phantom even when their positions are not ideally located. Our algorithm accurately segmented the objects within all three types of Catphan phantoms, i.e. CTP 500, CTP 504, and CTP 604. It automatically generated CT number linearity graphs to facilitate further assessment.

We found that measured values for Teflon and Delrin were 30-80 HU above the recommended limits. And Bone-20% values in Catphan 604 a little low, about 3 HU lower than the minimum of the recommended range, as was air in Catphan 500. The CT numbers for the other materials were all within range. Garayoa *et al.* [35] examined the Catphan 600 phantom with a Varian OBI CBCT and found that Teflon was about 60 HU above the reference value, while other materials were less than 35 HU from the recommended range. Won *et al.* [36] using a Varian Truebeam Linac found that Teflon and Delrin™ in the Catphan 504 phantom had a significant difference with a *p-value* <0.05 as a consequence of increasing the tube current above the head and chest protocol.

Obtaining a CT number similar to the reference is quite tricky, especially for materials with high density. This is because the probability of Compton scatter increases in materials with high densities. In the Catphan phantom, the insert size, which is relatively small in high-density materials such as Delrin, Teflon, and Bone-20%, cannot accommodate the scatter radiation. This results in a dramatic difference in the CT number values obtained for these materials from the manufacturer's reference values [37-40]. Studies

(Hatton [45], Guang [46]) revealed that the difference between measurement and reference could be up to 260 HU, depending on the scatter volume length. This explains why the CT number linearity often fails to pass the standard, as in Catphan 604. Materials with a lower density are more likely to result in accurate CT numbers.

Although deviation in CT number does not have a significant impact on the radiation dose [45,46], it does carry the risk of misdiagnosing patients when using QCT. The situation requires periodic monitoring of the CT scanner performance in producing an accurate CT number. Institute of Physics and Engineering in Medicine (IPEM) recommends measuring water and a high-density material such as Teflon in daily or weekly testing. Annual quality control can include materials other than these two [47]. It is recommended that quality control should be carried out with several variations that affect the output CT number, such as tube voltage, reconstruction algorithm, and slice thickness [48-50].

This study has some limitations. The algorithm was tested on a limited number of Catphan phantoms, namely Catphan 500, Catphan 504, and Catphan 604. There are other types of Catphan phantom such as Catphan 600 and Catphan 704 which were not included in this software. Also, the current software has not been compared with other software. Testing the algorithm with more phantoms and a comparison with other existing software needs to be done in the future to fully test the performance of this algorithm.

4.0 CONCLUSION

Our algorithm has successfully measured CT number linearity on three types of Catphan phantoms, i.e. Catphan 500, Catphan 504, and Catphan 604, quickly and accurately. Two phantoms, Catphan 500 and

504, yielded pass results ($R^2 > 0.99$) while the Catphan 604 was out of the tolerance limit. We found that higher density materials are more likely to result in CT numbers different from the reference values.

Conflicts of Interest

The author(s) declare(s) that there is no conflict of interest regarding the publication of this paper.

Acknowledgement

References

[1] Pola, A., Corbella, D., Righini, A., Torresin, A., Colombo, P. E., Vismara, L., Trombetta, L., Maddalo, M., Introini, M. V., Tinelli, D., Strohmenger, L., Garattini, G., Munari, A., & Triulzi, F. 2018. Computed Tomography Use in a Large Italian Region: Trend Analysis 2004-2014 of Emergency and Outpatient CT Examinations in Children and Adults. *European Radiology*. 28(6): 2308-2318.

[2] Kim, N. T., Kwon, S. S., Park, M. S., Lee, K. M., & Sung, K. H. 2022. National Trends in Pediatric CT Scans in South Korea: A Nationwide Cohort Study. *Taehan Yongsang Uihakhoe chi*. 83(1): 138-148.

[3] Huang, C. C., Effendi, F. F., Kosik, R. O., Lee, W. J., Wang, L. J., Juan, C. J., & Chan, W. P. 2023. Utilization of CT and MRI Scanning in Taiwan, 2000-2017. *Insights into Imaging*. 14(1): 23.

[4] Smith-Bindman, R., Kwan, M. L., Marlow, E. C., Theis, M. K., Bolch, W., Cheng, S. Y., Bowles, E. J. A., Duncan, J. R., Greenlee, R. T., Kushi, L. H., Pole, J. D., Rahm, A. K., Stout, N. K., Weinmann, S., & Miglioretti, D. L. 2019. Trends in Use of Medical Imaging in US Health Care Systems and in Ontario, Canada, 2000-2016. *JAMA*. 322(9): 843-856.

[5] Kwan, M. L., Miglioretti, D. L., Marlow, E. C., Aiello Bowles, E. J., Weinmann, S., Cheng, S. Y., Deosaransingh, K. A., Chavan, P., Moy, L. M., Bolch, W. E., Duncan, J. R., Greenlee, R. T., Kushi, L. H., Pole, J. D., Rahm, A. K., Stout, N. K., Smith-Bindman, R., & Radiation-Induced Cancers Study Team. 2019. Trends in Medical Imaging During Pregnancy in the United States and Ontario, Canada, 1996 to 2016. *JAMA Network Open*. 2(7): e197249.

[6] Seeram E. 2018. Computed Tomography: A Technical Review. *Radiologic Technology*. 89(3): 279CT-302CT.

[7] Seeram E. 2014. Computed Tomography Dose Optimization. *Radiologic Technology*. 85(6): 655CT-675CT.

[8] Alresheedi, N., Walton, L., Hogg, P., Webb, J., & Tootell, A. 2021. Evaluation of X-ray Table Mattresses for Radiation Attenuation and Impact on Image Quality. *Radiography (London, England: 1995)*. 27(1): 215-220.

[9] Ma, X., Figl, M., Unger, E., Buschmann, M., & Homolka, P. 2022. X-ray Attenuation of Bone, Soft and Adipose Tissue in CT from 70 to 140 kV and Comparison with 3D Printable Additive Manufacturing Materials. *Scientific Reports*. 12(1): 14580.

[10] Kunert, P., Trinkl, S., Giussani, A., Reichert, D., & Brix, G. 2022. Tissue Equivalence of 3D Printing Materials with Respect to Attenuation and Absorption of X-rays used for Diagnostic and Interventional Imaging. *Medical Physics*. 49(12): 7766-7778.

[11] DenOtter TD, Schubert J. Hounsfield Unit. [Updated 2023 Mar 6]. In: StatPearls [Internet]. Treasure Island (FL): StatPearls Publishing.

[12] Ai, H. A., Meier, J. G., & Wendt, R. E. 2018. HU Deviation in Lung and Bone Tissues: Characterization and a Corrective Strategy. *Medical Physics*. 45(5): 2108-2118.

[13] Levine, Z. H., Peskin, A. P., Holmgren, A. D., & Garboczi, E. J. 2018. Preliminary X-ray CT Investigation to Link Hounsfield Unit Measurements with the International System of Units (SI). *PloS One*. 13(12): e0208820.

[14] Egashira, R., & Raghu, G. 2022. Quantitative Computed Tomography of the Chest for Fibrotic Lung Diseases: Prime Time for Its Use in Routine Clinical Practice? *Respirology (Carlton, Vic.)*. 27(12): 1008-1011.

[15] Ito, K., Kondo, T., Andreu-Arasa, V. C., Li, B., Hirahara, N., Muraoka, H., Sakai, O., & Kaneda, T. 2022. Quantitative Assessment of the Maxillary Sinusitis using Computed Tomography Texture Analysis: Odontogenic vs Non-odontogenic Etiology. *Oral Radiology*. 38(3): 315-324.

[16] Zhou, G., Li, F., Wang, K., Lin, X., & Yu, X. 2020. Research on a Quantitative Method for Three-dimensional Computed Tomography of Chemiluminescence. *Applied Optics*. 59(17): 5310-5318.

[17] Title, R. S., Harper, K., Nelson, E., Evans, T., Tello R. 2005. Observer Performance in Assessing Anemia on Thoracic CT. *AJR Am J Roentgenol*. 185(5): 1240-1244.

[18] Jung, C., Groth, M., Bley, T. A., Henes, F. O., Treszl, A., Adam, G., & Bannas, P. 2012. Assessment of Anemia during CT Pulmonary Angiography. *European Journal of Radiology*. 81(12): 4196-4202.

[19] Zhou, Q. Q., Yu, Y. S., Chen, Y. C., Ding, B. B., Fang, S. Y., Yang, X., Zhang, B., & Zhang, H. 2018. Optimal Threshold for the Diagnosis of Anemia Severity on Unenhanced Thoracic CT: A Preliminary Study. *European Journal of Radiology*. 108: 236-241.

[20] Kwan, A. C., Gransar, H., Tzolos, E, *et al*. Kwan, A. C., Gransar, H., Tzolos, E., Chen, B., Otaki, Y., Klein, E., Pope, A. J., Han, D., Howarth, A., Jain, N., Dey, D., Miller, R. J., Cheng, V., Azarbal, B., & Berman, D. S. 2021. The Accuracy of Coronary CT Angiography in Patients with Coronary Calcium Score above 1000 Agatston Units: Comparison with Quantitative Coronary Angiography. *Journal of Cardiovascular Computed Tomography*. 15(5): 412-418.

[21] Gatti, M., Gallone, G., Poggi, V., Bruno, F., Serafini, A., Depaoli, A., De Filippo, O., Conrotto, F., Darvizeh, F., Faletti, R., De Ferrari, G. M., Fonio, P., & D'Ascenzo, F. 2022. Diagnostic Accuracy of Coronary Computed Tomography Angiography for the Evaluation of Obstructive Coronary Artery Disease in Patients Referred for Transcatheter Aortic Valve Implantation: A Systematic Review and Meta-Analysis. *European Radiology*. 32(8).

[22] Guan, X., Yao, L., Tan, Y., Shen, Z., Zheng, H., Zhou, H., Gao, Y., Li, Y., Ji, W., Zhang, H., Wang, J., Zhang, M., & Xu, X. 2021. Quantitative and Semi-quantitative CT Assessments of Lung Lesion Burden in COVID-19 Pneumonia. *Scientific Reports*. 11(1): 5148.

[23] Lu, W., Wei, J., Xu, T., Ding, M., Li, X., He, M., Chen, K., Yang, X., She, H., & Huang, B. 2021. Quantitative CT for Detecting COVID-19 Pneumonia in Suspected Cases. *BMC Infectious Diseases*. 21(1): 836.

[24] Zhang, K., Liu, X., Shen, J., Li, Z., Sang, Y., Wu, X., Zha, Y., Liang, W., Wang, C., Wang, K., Ye, L., Gao, M., Zhou, Z., Li, L., Wang, J., Yang, Z., Cai, H., Xu, J., Yang, L., Cai, W., … Wang, G. (2020). Clinically Applicable AI System for Accurate Diagnosis, Quantitative Measurements, and Prognosis of COVID-19 Pneumonia Using Computed Tomography. *Cell*. 182(5): 1360.

[25] Thakur, S. K., Singh, D. P., & Choudhary, J. 2020. Lung Cancer Identification: A Review on Detection and Classification. *Cancer Metastasis Reviews*. 39(3): 989-998.

[26] Mehnati, P., Jafari, T. M., & Ghavami, M. 2020. CT Role in the Assessment of Existence of Breast Cancerous Cells. *Journal of Biomedical Physics & Engineering*. 10(3): 349-356.

[27] Suyudi, I., Anam, C., Sutanto, H., Triadyaksa, P., & Fujibuchi, T. 2020. Comparisons of Hounsfield Unit Linearity between Images Reconstructed using an Adaptive Iterative Dose Reduction (AIDR) and a Filter Back-Projection (FBP) Techniques. *Journal of Biomedical Physics & Engineering*. 10(2): 215-224.

[28] Roa, A. M., Andersen, H. K., & Martinsen, A. C. 2015. CT Image Quality Over Time: Comparison of Image Quality for Six Different CT Scanners Over a Six-year Period. *Journal of Applied Clinical Medical Physics*. 16(2): 4972.

[29] Nute, J. L., Rong, J., Stevens, D. M., Darensbourg, B. J., Cheng, J., Wei, W., Hobbs, B. P., & Cody, D. D. 2013. Evaluation of over 100 Scanner-years of Computed Tomography Daily Quality Control Data. *Medical Physics*. 40(5): 051908.

[30] Alikhani, B., Jamali, L., Raatschen, H. J., Wacker, F., & Werncke, T. 2017. Impact of CT Parameters on the Physical Quantities Related to Image Quality for Two MDCT Scanners using the ACR Accreditation Phantom: A Phantom Study. *Radiography (London, England: 1995)*. 23(3): 202-210.

[31] Mansour, Z., Mokhtar, A., Sarhan, A., Ahmed, M. T., El-Diasty, T. 2016. Quality Control of Image using American College of Radiology (ACR) Phantom. *Egypt J Radiol Nucl Med*. 47(4): 1665-1671.

[32] Nowik, P., Bujila, R., Poludniowski, G., & Fransson, A. 2015. Quality Control of CT Systems by Automated Monitoring of Key Performance Indicators: A Two-Year Study. *Journal of Applied Clinical Medical Physics*. 16(4): 254-265.

[33] An, H. J., Son, J., Jin, H., Sung, J., Chun, M. 2019. Acceptance Test and clinical commissioning of CT simulator. *Prog Med Phys*. 30(4): 160

[34] Njiki, C. , Ndjaka Manyol, J. , Ebele Yigbedeck, Y. , Abou'ou, D., Yimele, B. and Sabouang, J. 2018. Assessment of Image Quality Parameters for Computed Tomography in the City of Yaoundé. *Open Journal of Radiology*. 8: 37-44.

[35] Garayoa, J., & Castro, P. 2013. A Study on Image Quality Provided by a Kilovoltage Cone-beam Computed Tomography. *Journal of Applied Clinical Medical Physics*. 14(1): 3888.

[36] Won, H. S., Chung, J. B., Choi, B. D., Park, J. H., & Hwang, D. G. 2016. Accuracy of Automatic Matching of Catphan 504 Phantom in Cone-beam Computed Tomography for Tube Current-exposure Time Product. *Journal of Applied Clinical Medical Physics*. 17(6): 421-428.

[37] The Phantom Laboratory. Smari Image Analysis. https://www.phantomlab.com/smari-image-analysis.

[38] QA Benchmark. AutoQA Plus CT. http://qabenchmark.com/ct/.

[39] Karius, A., & Bert, C. 2022. QAMaster: A New Software Framework for Phantom-based Computed Tomography Quality Assurance. *Journal Of Applied Clinical Medical Physics*. 23(4): e13588.

[40] Standard Imaging. QA Pilot. https://www.standardimaging.com/products/qa-pilot-with-pipspro-autopilot.

[41] Medical Physics Perth. CT Quality Inspector. https://www.medicalphysicsperth.com/ct-quality-inspector-ctqi.

[42] Anam, C., Naufal, A., Fujibuchi, T., Matsubara, K., & Dougherty, G. 2022. Automated Development of the Contrast-detail Curve based on Statistical Low-contrast Detectability in CT Images. *Journal of Applied Clinical Medical Physics*. 23(9): e13719.

[43] Anam, C., Amilia, R., Naufal, A., Budi, W. S., Maya, A. T., & Dougherty, G. 2022. The Automated Measurement of CT Number Linearity using an ACR Accreditation Phantom. *Biomedical Physics & Engineering Express*. 9(1): 10.1088/2057-1976/aca9d5.

[44] Regulation of the nuclear energy supervisory agency of the Republic of Indonesia number 2 concerning the conformity test of diagnostic and interventional radiology x-ray machine *Nuclear Energy Regulatory Agency of Indonesia* 2018.

[45] Hatton, J., McCurdy, B., & Greer, P. B. 2009). Cone Beam Computerized Tomography: The Effect of Calibration of the Hounsfield Unit Number to Electron Density on Dose Calculation Accuracy for Adaptive Radiation Therapy. *Physics in Medicine and Biology*. 54(15): N329-N346.

[46] Guan, H., & Dong, H. 2009. Dose Calculation Accuracy using Cone-beam CT (CBCT) for Pelvic Adaptive Radiotherapy. *Physics in Medicine and Biology*. 54(20): 6239-6250.

[47] Institute of Physics and Engineering in Medicine. 2003. Measurements of the Performance Characteristics of Diagnostic x-ray Systems Used in Medicine. Part III. Computed Tomography x-ray Scanners. IPEM Report 32. 2nd ed. York: IPEM. 2003: 1-98.

[48] Afifi, M. B., Abdelrazek, A., Deiab, N. A., Abd El-Hafez, A. I., El-Farrash, A. H. 2020. The Effects of CT x-ray Tube Voltage and Current Variations on the Relative Electron Density (RED) and CT Number Conversion Curves. *Journal of Radiation Research and Applied Sciences*. 13(1): 1-11.

[49] Ohno, Y., Fujisawa, Y., Fujii, K., Sugihara, N., Kishida, Y., Seki, S., & Yoshikawa, T. 2019. Effects of Acquisition Method and Reconstruction Algorithm for CT Number Measurement on Standard-dose CT and Reduced-dose CT: A QIBA Phantom Study. *Japanese Journal of Radiology*. 37(5): 399-411.

[50] Gierada, D. S., Bierhals, A. J., Choong, C. K., Bartel, S. T., Ritter, J. H., Das, N. A., Hong, C., Pilgram, T. K., Bae, K. T., Whiting, B. R., Woods, J. C., Hogg, J. C., Lutey, B. A., Battafarano, R. J., Cooper, J. D., Meyers, B. F., & Patterson, G. A. 2010. Effects of CT Section Thickness and Reconstruction Kernel on Emphysema Quantification Relationship to the Magnitude of the CT Emphysema Index. *Academic Radiology*. 17(2): 146-156.